

Coulomb problem in momentum space without screening

N. J. Upadhyay,^{1,*} V. Eremenko,^{2,5,†} L. Hlophe,² F. M. Nunes,^{1,‡} Ch. Elster,^{2,§} G. Arbanas,³ J. E. Escher,⁴ and I. J. Thompson⁴
(TORUS Collaboration)

¹*National Superconducting Cyclotron Laboratory and Department of Physics and Astronomy, Michigan State University, East Lansing, Michigan 48824, USA*

²*Institute of Nuclear and Particle Physics and Department of Physics and Astronomy, Ohio University, Athens, Ohio 45701, USA*

³*Reactor and Nuclear Systems Division, Oak Ridge National Laboratory, Oak Ridge, Tennessee 37831, USA*

⁴*Lawrence Livermore National Laboratory, L-414, Livermore, California 94551, USA*

⁵*D.V. Skobel'syn Institute of Nuclear Physics, M.V. Lomonosov Moscow State University, Moscow, 119991, Russia*

(Received 1 May 2014; published 28 July 2014)

Background: The repulsive Coulomb force poses severe challenges when solving the three-body problem for (d, p) reactions on intermediate mass and heavy nuclei. Recently, a new approach based on the Coulomb-distorted basis in momentum space was proposed.

Purpose: In this work, we demonstrate the feasibility of using the Coulomb-distorted basis in momentum space for calculating matrix elements expected in a wide range of nuclear reactions.

Method: We discuss the analytic forms of the Coulomb wave function in momentum space. We analyze the singularities in the Coulomb-distorted form factors and the required regularization techniques. Employing a separable interaction derived from a realistic nucleon-nucleus optical potential, we compute and study the Coulomb-distorted form factors for a wide range of cases, including charge, angular momentum, and energy dependence. We also investigate in detail the precision of our calculations.

Results: The Coulomb-distorted form factors differ significantly from the nuclear form factors except for the very highest momenta. Typically, the structure of the form factor is shifted away from zero momentum due to the Coulomb interaction. Unlike the Yamaguchi forms typically used in three-body methods, our realistic form factors have a short high-momentum tail, which allows for a safe and efficient truncation of the momentum grid.

Conclusions: Our results show that the Coulomb-distorted basis can be effectively implemented.

DOI: [10.1103/PhysRevC.90.014615](https://doi.org/10.1103/PhysRevC.90.014615)

PACS number(s): 24.10.-i, 25.40.Cm, 25.45.Hi, 21.30.Fe

I. INTRODUCTION

Nuclear reactions are an important probe into the structure of unstable nuclei. In particular, light probes offer a diverse range of applicability, allowing us to explore shell evolution, collectivity, and electromagnetic processes and to extract astrophysical rates that are not directly accessible [1]. Among the light probes, deuteron-induced reactions are particularly attractive from an experimental perspective (since deuterated targets are readily available and cross sections are often advantageous), but also from a theoretical perspective, because the scattering problem can then be reduced to an effective three-body problem [2]. Although deuteron-induced single-nucleon transfer (d, p) reactions have been traditionally used to study shell structure in stable nuclei, experimental techniques have been developed to apply the same approaches to exotic beams (e.g., [3]). Deuteron-induced (d, p) or (d, n) reactions in inverse kinematics are also useful for extracting neutron or proton capture rates on unstable nuclei of astrophysical relevance (e.g., [4]). Given the many ongoing experimental programs worldwide using these reactions, a reliable reaction theory for (d, p) reactions is critical.

One of the most challenging aspects of solving the three-body problem for nuclear reactions is the repulsive Coulomb interaction. While the Coulomb interaction for light nuclei is often a small correction to the problem, this is certainly not the case for intermediate-mass and heavy systems [5]. Over the last decade, many theoretical efforts have focused on advancing the theory for (d, p) reactions (e.g., [6,7]) and testing existing methods (e.g., [2,8,9]). Currently, the most complete implementation of the theory is provided by the Lisbon group [10], who solve the Faddeev equations in the Alt, Grassberger, and Sandhas (AGS) [11] formulation. The method introduced in [10] treats the Coulomb interaction with a screening and renormalization procedure as detailed in [12,13]. While the current implementation of the Faddeev-AGS equations with screening is computationally effective for light systems, as the charge of the nucleus increases technical difficulties arise in the screening procedure [5]. Indeed, for most of the new exotic nuclei to be produced at the Facility of Rare Isotope Beams, the current method is not adequate. One then has to explore solutions to the nuclear reaction three-body problem where the Coulomb problem is treated without screening.

In Ref. [6], a three-body theory for (d, p) reactions is derived with explicit inclusion of target excitations, where no screening of the Coulomb force is introduced. Therein, the Faddeev-AGS equations are cast in the Coulomb-distorted partial-wave representation, instead of the plane-wave basis. In [6], a first term of this basis (for $l = 0$) is derived for a

*neelam@phys.lsu.edu

†eremenko@ohio.edu

‡nunes@nscl.msu.edu

§elster@ohio.edu

Yamaguchi interaction, for which there is an analytic solution. For a practical implementation of the theory of [6], one needs to be able to accurately compute the Coulomb-distorted form factors used in the theory. In this work we generalize the approach introduced in [6] to arbitrary angular momenta and for nonanalytic complex interactions. After the form factors have been obtained, the full Faddeev-AGS equations should be solvable without screening, and from the resulting t matrices, the transfer cross sections can be obtained.

Coulomb-distorted form factors in momentum space have been considered before [14–16]. In Ref. [14] the authors discuss the schematics on how to include the Coulomb interaction in nuclear reactions, making use of the closed analytic form for the Coulomb wave function in momentum space. More details on the mathematical difficulties can be found in [15] and a couple of practical calculations for proton-proton scattering are available in [16].

The Padova group [17,18] introduced a rank-1 separable interaction to represent the nuclear force up to a few MeV and made use of the Coulomb-distorted basis to compute proton elastic scattering on light nuclei. Our approach has similarities with the work of the Padova group [17,18]. However, whereas that group uses low-rank real Yamaguchi forms, our conviction is that the nuclear form factors should reflect the density distribution of the nucleus. Our implementation can handle nonanalytic forms of the separable interactions, and our applications make use of the separable complex nuclear form factors developed in [19]. In that work, a separable representation of a global realistic nucleon-nucleus optical potential, of Woods-Saxon form, is performed by using a generalization of the Ernst, Shakin, and Thaler (EST) scheme for non-Hermitian interactions. Since we are interested in processes around tens of MeV, a rank-1 separable interaction is seriously insufficient (note that in [19] rank-5 interactions were required for some partial waves). Because our ultimate goal is to insert this basis in the Faddeev-AGS equations, particular attention is paid to the computational efficiency of the methods.

Expectation values with Coulomb wave functions in momentum space are also considered in Ref. [20]. Their calculations are performed in three dimensions, instead of using a partial-wave representation. Furthermore, the singularity that occurs when integrating over a Coulomb wave function is not explicitly treated on the real axis, but rather on a path in the complex plane. The value on the real axis is then obtained by an iterative procedure based on continued fractions. As discussed in Sec. II, and in contrast with [20], in our approach we use partial wave decomposition as well as integration along the real axis.

In this work, we will discuss the challenges of implementing the Coulomb-distorted basis in momentum space for the realistic nucleon-nucleus case. In Sec. II, we provide the theoretical framework with supplementary information gathered in Appendices A and B. Coulomb-distorted form factors are discussed in Sec. III, where we first show results for the rank-1 Yamaguchi test case (Sec. III A), followed by a detailed study of the Coulomb-distorted form factors for realistic cases (Sec. III B). Our results cover a wide variety of cases, including charge dependence, angular momentum

dependence, as well as incident energy dependence. Finally, in Sec. IV, we summarize our findings and discuss our results.

II. THEORETICAL FRAMEWORK

In order to treat charged-particle scattering in momentum space without employing a screening procedure for the Coulomb force, it is possible to formulate the scattering problem in a momentum-space Coulomb basis instead of a plane-wave basis. This was proposed in Ref. [6] for the generalized Faddeev-AGS equations in which two of the three particles have charge. In order for such an approach to be numerically practical, one needs reliable techniques to calculate expectation values in this basis.

Thus, the starting point is the analytic expression for the Coulomb wave function in momentum space, which, after a partial-wave decomposition, can be written as (see [21] and Appendix A)

$$\psi_{l,p}^C(q) = -\frac{2\pi e^{\eta\pi/2}}{pq} \lim_{\gamma \rightarrow +0} \frac{d}{d\gamma} \left\{ \left[\frac{q^2 - (p + i\gamma)^2}{2pq} \right]^{i\eta} \times (\zeta^2 - 1)^{-i\frac{\eta}{2}} Q_l^{i\eta}(\zeta) \right\}. \quad (1)$$

Here, p is the magnitude of a fixed asymptotic momentum and $\zeta = (p^2 + q^2 + \gamma^2)/2pq$. The Sommerfeld parameter is given as $\eta = Z_1 Z_2 e^2 \mu / p$, where Z_1 and Z_2 are the charges of the two bodies involved and μ is the reduced mass of the two-body system under consideration. The spherical function $Q_l^{i\eta}(\zeta)$ in Eq. (1) can be expressed in terms of hypergeometric functions ${}_2F_1$ [14]; however, care must be taken in its evaluation, since there are specific limits of validity of the various expansions. Specific difficulties together with the expressions implemented in this work are discussed in detail in Appendix A.

When carrying out calculations in a momentum-space Coulomb basis, it is necessary to evaluate matrix elements of operators in this basis. In general, such operators can be functions of different momenta p and p' related to the bra- and ket basis vectors. When expressing the Faddeev-AGS equations in the Coulomb basis as in Ref. [6], the operators for the interactions in the two-body subsystems are assumed to be of separable form. In this case, the evaluation of matrix elements consists of integrals over the Coulomb wave function and a smooth function (real or complex valued) of a single momentum representing the nuclear operator (form factor).

These nuclear form factors should be chosen according to the physical properties of the two-body system under consideration. While for the neutron-proton interaction traditionally a superposition of Yamaguchi form factors is used [22,23], one cannot expect the same form to be valid for describing the nucleon-nucleus interaction. Indeed, phenomenological optical potentials have Woods-Saxon forms. Recently, we developed separable representations for optical potentials based on a generalization of the EST scheme for complex potentials [19]. These representations of up to rank 5 for nuclei

as heavy as ^{208}Pb are phase equivalent to the optical potentials based on Woods-Saxon parametrizations (in our case the CH89 global phenomenological optical potential [24]).

The separable partial-wave t -matrix operator for a fixed energy E given in Ref. [19] has the form

$$t_l(E) = \sum_{i,j} u |f_{l,k_{E_i}}\rangle \tau_{ij}(E) \langle f_{l,k_{E_j}}^* | u, \quad (2)$$

where $f_{l,k_{E_i}}$ is the unique regular radial wave function corresponding to a complex potential u and asymptotic energy $E_i = \hbar^2 k_{E_i}^2 / (2\mu)$ (where μ is the reduced mass), and $f_{l,k_{E_j}}^*$ is the unique regular radial wave function corresponding to u^* . This choice is necessary to preserve time-reversal symmetry in case of complex potentials, as discussed in [19]. Evaluating its momentum-space matrix elements $\langle p | t_l(E) | p' \rangle$ in a plane-wave basis gives the nuclear form factors

$$\begin{aligned} \langle p | u | f_{l,k_E} \rangle &= t_l(p, k_E; E_{k_E}) \equiv u_l(p), \\ \langle f_{l,k_E}^* | u | p' \rangle &= t_l(p', k_E; E_{k_E}) \equiv u_l(p'), \end{aligned} \quad (3)$$

where the $t_l(p, k_E; E_{k_E})$ are the half-shell two-body t matrices obtained as a solution of a momentum-space Lippmann-Schwinger equation with the complex potential u .

The corresponding Coulomb-distorted form factors are obtained by replacing the plane-wave basis state by a Coulomb basis state $|\psi_{l,p}^C\rangle$, leading to

$$\langle \psi_{l,p}^C | u | f_{l,k_E} \rangle = \int_0^\infty \frac{dq q^2}{2\pi^2} u_l(q) \psi_{l,p}^C(q)^* \equiv u_l^C(p), \quad (4)$$

$$\langle f_{l,k_E}^* | u | \psi_{l,p}^C \rangle = \int_0^\infty \frac{dq q^2}{2\pi^2} u_l(q) \psi_{l,p}^C(q) \equiv u_l^C(p)^\dagger. \quad (5)$$

When $\eta \rightarrow 0$, Eqs. (4) and (5) tend to Eq. (3).

Equations (4) and (5) are a generalization of the form introduced in Ref. [6] to account for complex interactions. In [6], $u_l^C(p)$ was obtained for $l=0$ and a rank-1 real Yamaguchi interaction. In that case, an analytic expression for the integral of Eq. (4) can be derived. We will mostly concentrate on presenting results obtained with the complex optical potentials developed in [19]. For the sake of numerically testing our approach, we will also present calculations based on Yamaguchi-type form factors.

The main challenge in computing the integrals of Eq. (4) is the oscillatory singularity in the integrand for $q = p$, which is of the form

$$S(q-p) = \lim_{\gamma \rightarrow +0} \frac{1}{(q-p+i\gamma)^{1+i\eta}}. \quad (6)$$

This type of singularity cannot be numerically evaluated by using the familiar principal value subtractions but rather needs to be treated by using the scheme of Gel'fand and Shilov [25], as proposed in [6,14]. In Appendix B, we discuss the nature of the singularity and present a generalization of the regularization scheme of [6] adequate for complex form factors, a critical point in this work. The essence of the Gel'fand and Shilov scheme is to subtract as many terms as needed of the Laurent expansion in a small region around the pole so that the oscillations around the pole become small, and the integral becomes regular. We want to point out that our

numerical calculations are entirely performed along the real axis, in contrast to the approach chosen in Ref. [20].

III. THE COULOMB-DISTORTED FORM FACTORS

To our knowledge, this work represents the first attempt to numerically obtain Coulomb-distorted matrix elements for realistic nucleon-nucleus interactions where the nucleus has a relatively large charge. Given the challenge of accurately calculating the partial-wave Coulomb wave functions as well as handling their oscillating singularity, it is critical to demonstrate the numerical accuracy of our computations $u_l^C(p)$ of Eq. (4). For this reason we first study the Coulomb-distorted nuclear form factors for the separable Yamaguchi interaction as used in Refs. [6,18] before turning to form factors derived from Woods-Saxon interactions. In all our final results below, we used the two-term regularization technique of Appendix B.

A. Tests with a Yamaguchi form factor

Using a Yamaguchi form factor as a test case has the advantage that calculations can be performed not only numerically but also semianalytically, in our case using the MATHEMATICA[®] [26] software. The Coulomb-distorted form factors $u_l^{C,Y}(p)$, calculated as an integral over the Coulomb wave function given in Eq. (1), and the Yamaguchi form factor from [6] are depicted in Fig. 1, where our numerical results (labeled FortY) are compared with those produced by MATHEMATICA[®] [26] (labeled MathY). The top panels (a) and (b) concern protons on ^{12}C and the bottom panels (c) and (d) refer to protons on ^{208}Pb . On the left (right) we show the real (imaginary) parts of $u_l^{C,Y}(p)$. Both $l=0$ and $l=4$ are shown.

There are a number of general features that can immediately be highlighted. The stronger the Coulomb interaction is, the

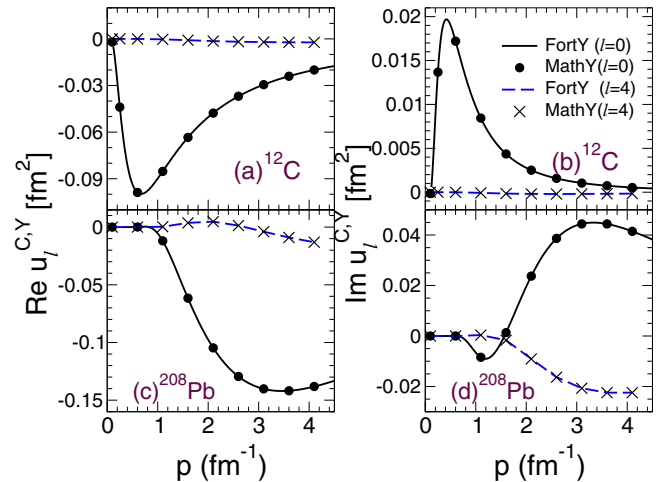


FIG. 1. (Color online) The partial-wave Coulomb form factors $u_l^C(p)$ obtained with a Yamaguchi interaction as a function of the external momentum p for selected angular momenta l . Comparison between our numerical evaluation (solid lines) and the MATHEMATICA[®] [26] results (symbols): (a) real part $u_l^C(p)$ for $p + ^{12}\text{C}$; (b) imaginary part of $u_l^C(p)$ for $p + ^{12}\text{C}$; (c) real part $u_l^C(p)$ for $p + ^{208}\text{Pb}$; (d) imaginary part of $u_l^C(p)$ for $p + ^{208}\text{Pb}$.

larger the shift of the distribution away from $p = 0$. This shift is clearly most pronounced for large-charge targets, such as $Z = 82$ for ^{208}Pb . As expected, $u_l^{C,Y}(p)$ follows a normal hierarchy; the higher partial waves decrease in magnitude compared to the lower partial waves, providing good convergence properties when computing observables. Since the Coulomb functions are real functions multiplied by $e^{i\sigma_l}$ (see Appendix B 2) and the Yamaguchi form factor is also a real function of the momentum p , the real parts of $u_l^{C,Y}(p)$ contain essentially the same information as the imaginary parts. A characteristic feature of the Yamaguchi form factors is a slow fall-off for large momenta, which is a consequence of the behavior of the Yukawa interaction at $r = 0$. Thus, Coulomb-distorted form factors extend out to large momentum (as far as 10 fm^{-1} in the case of ^{208}Pb). In order to perform a meaningful comparison between the numerical and semianalytical calculations, we concentrate on the behavior of the form factor in the window $p \in [0, 4] \text{ (fm}^{-1}\text{)}$, where the obtained $u_l^{C,Y}(p)$ reach their maximum values. Indeed, as we shall see in Sec. III B, realistic form factors fall off much faster as a function of p than the Yamaguchi ones, and in this comparison we prefer to concentrate on the relevant momentum regions.

Given the numerical difficulties involved in computing the Coulomb-distorted basis, we would like to address the accuracy of our calculations. We first compared the accuracy of our numerical implementation of the Coulomb wave functions with the corresponding results provided by MATHEMATICA[®]. The agreement found was on the order of 10 significant digits. Next, we compared the accuracy of the integration given by Eq. (4) and found that our numerical calculation agreed with the corresponding MATHEMATICA[®] calculation for about six significant figures. As shown in Fig. 1, the Coulomb-distorted Yamaguchi form factors obtained with our numerical implementation (lines) agree perfectly with the results obtained with MATHEMATICA[®] (symbols). This demonstrates that our numerical implementation of the Coulomb wave functions, the integration, and regularization techniques, as discussed in Appendix B, provides a reliable method for calculating form factors involving Coulomb wave functions in momentum space.

In order to explore the importance of the region around the singularity, we have performed additional calculations where we removed a region $q \in [p - \Delta, p + \Delta]$ around the pole $q = p$ from the integral of Eq. (4). In Fig. 2 we show the fractional contribution from the pole, namely, the absolute value of the relative difference between the results $u_l^{C,Y}(p, \Delta)$, obtained by removing the pole region, and the full integral $u_l^{C,Y}(p)$, i.e., the quantity

$$\mathbf{D}(\Delta) = \frac{|u_l^{C,Y}(p) - u_l^{C,Y}(p, \Delta)|}{|u_l^{C,Y}(p)|}, \quad (7)$$

for fixed values of p . We choose $p = 0.6 \text{ fm}^{-1}$ (with center-of-mass energy $E_{\text{c.m.}} = 8.1 \text{ MeV}$) for ^{12}C and $p = 1.1 \text{ fm}^{-1}$ (with center-of-mass energy $E_{\text{c.m.}} = 7.5 \text{ MeV}$) for ^{208}Pb , as examples. For each of these values of p , the nuclear form factor is far from any node. In Fig. 2 the calculations of the above defined quantity $\mathbf{D}(\Delta)$ are shown as function of Δ for $p + ^{12}\text{C}$ in panel (a) and for $p + ^{208}\text{Pb}$ in panel (b) for the

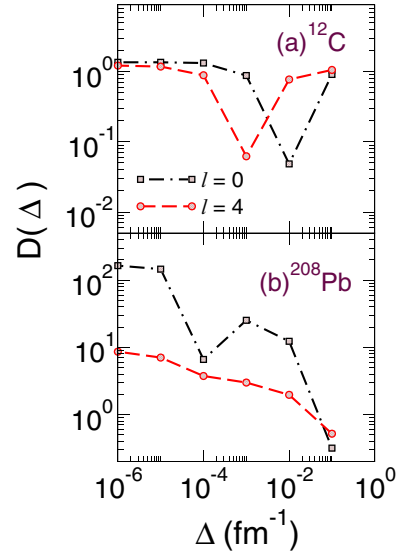


FIG. 2. (Color online) The fractional contribution of the pole $\mathbf{D}(\Delta)$ for the Yamaguchi form factors of Fig. 1 at specific momenta: (a) $p + ^{12}\text{C}$ at $p = 0.6 \text{ fm}^{-1}$ and (b) $p + ^{208}\text{Pb}$ at $p = 1.1 \text{ fm}^{-1}$. Shown are $l = 0$ (dot-dashed line) and $l = 4$ (dashed line) partial waves.

$l = 0$ (dot-dashed lines) and $l = 4$ (dashed lines). In case of ^{12}C we find that the relative difference is always around 10% or larger, independent of the Δ used and independent of the partial wave. As expected, the situation for ^{208}Pb is worse; discrepancies are about two orders of magnitude for $l = 0$ and one order of magnitude for $l = 4$. The demonstration given in Fig. 2 emphasizes the importance of the pole region.

B. Coulomb-distorted form factors for nuclear optical potentials

When considering nucleon scattering off a heavy nucleus, a rank-1 Yukawa-type interaction is not suitable. Instead, the effective nucleon-nucleus interaction, usually referred to as the optical potential, is parametrized with Woods-Saxon forms and their derivatives (i.e., [24,27,28]). With this in mind, a separable representation based on Woods-Saxon-type optical potentials was derived in a generalized EST scheme [19], and nuclear form factors were obtained for a variety of nuclei. This separable interaction is better suited to describe the processes we are interested in. For ^{48}Ca and ^{208}Pb , we use the nuclear form factors presented in [19], which are based on the CH89 global optical potential [24]. For ^{12}C , we choose to compute nuclear form factors based on the Weppner-Penney phenomenological optical potential [27], which is valid in this mass region. Table I gives the support points used for the separable representation of the ^{12}C optical potential presented in this work. Within the framework of the EST-based separable potentials, the form factors $u_l(p)$ correspond to the half-shell t matrices calculated at given fixed scattering energies, namely, the EST support points.

After having established the numerical procedures to compute Coulomb-distorted form factors using a Yukawa-type function, we now turn to studying the Woods-Saxon

TABLE I. EST support points at center-of-mass energies E_{k_i} used for constructing the separable representation of the partial wave S matrix of the $n + {}^{12}\text{C}$ system described by the Weppner-Penney phenomenological optical potential [27].

	Partial wave(s)	Rank	EST support point(s) (MeV)
$n + {}^{12}\text{C}$	$l = 0, 1, 2, 3, 4$	4	4, 13, 30, 46
	$l = 5, 6$	3	12, 28, 46
	$l = 7, 8$	2	14, 32
	$l \geq 9$	1	28

type form factors. One difference here is that the latter are only given as tabulated functions, and thus they need to be interpolated during the integration process. The other is that the potentials have an imaginary part. The generalization of the regularization proposed in [6] for complex potentials is described in detail in Appendix B.

In Figs. 3 and 4 we present the real and imaginary parts of the nuclear form factor $u_l(p)$ (left panels) and the corresponding Coulomb-distorted nuclear form factors $u_l^C(p)$ (right panels) calculated according to Eq. (4). We show results for protons on ${}^{12}\text{C}$ [panels (a) and (b)], ${}^{48}\text{Ca}$ [panels

(c) and (d)], and ${}^{208}\text{Pb}$ [panels (e) and (f)] for different angular momenta. The form factor for ${}^{12}\text{C}$ corresponds to the fixed support point $E_{c.m.} = 30$ MeV, the one for ${}^{48}\text{Ca}$ to the support point $E_{c.m.} = 36$ MeV, and the one for ${}^{208}\text{Pb}$ to $E_{c.m.} = 36$ MeV (except for $l = 8$, where it is 39 MeV). The choice of the support points is dictated by the overall quality of the separable representation of the scattering amplitude for the corresponding system, and we made sure to use support points in the same energy range for our illustration.

Let us first turn our attention to the real parts of the form factors (Fig. 3). At zero momentum, the nuclear form factors are finite for $l = 0$ while going to zero as p^l for all higher angular momenta as dictated by the partial-wave decomposition of the two-body t matrix from which they are derived. In contrast, the Coulomb-distorted form factors are zero for $l = 0$ at $p = 0$. This is identical to the finding in Sec. III A and is associated with the existence of a repulsive barrier at the origin. Comparison of the left and right panels of Fig. 3 also shows that the Coulomb interaction generally pushes the structure of the form factors from lower momenta to higher momenta. In addition, we observe that the heavier the nucleus, the more structure the corresponding form factors exhibit. However, it is interesting to note that, for all nuclei

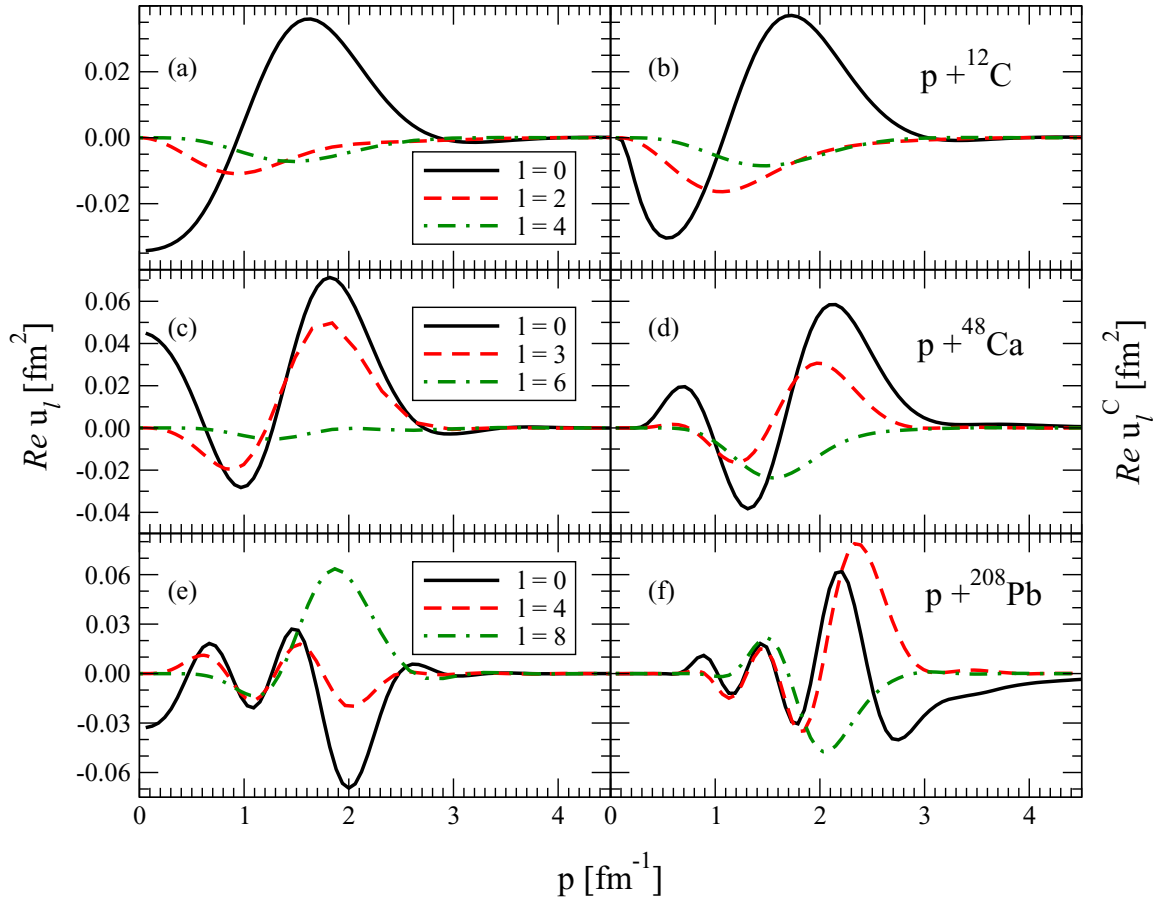


FIG. 3. (Color online) The real parts of the partial-wave nuclear form factors $u_l(p)$ (left panels) and the Coulomb-distorted nuclear form factors $u_l^C(p)$ (right panels) as function of the external momentum p for selected angular momenta l : (a) $\Re u_l(p)$ for $n + {}^{12}\text{C}$; (b) $\Re u_l^C(p)$ for $p + {}^{12}\text{C}$; (c) $\Re u_l(p)$ for $n + {}^{48}\text{Ca}$; (d) $\Re u_l^C(p)$ for $p + {}^{48}\text{Ca}$; (e) $\Re u_l(p)$ for $n + {}^{208}\text{Pb}$; (f) $\Re u_l^C(p)$ for $p + {}^{208}\text{Pb}$. The form factors for ${}^{12}\text{C}$ correspond to the fixed support point $E_{cm} = 30$ MeV, that for ${}^{48}\text{Ca}$ is at a fixed support point $E_{cm} = 36$ MeV, while the nuclear form factors for ${}^{208}\text{Pb}$ are at a fixed support point $E_{cm} = 36$ MeV for $l = 0, 4$ and $E_{cm} = 39$ MeV for $l = 8$.

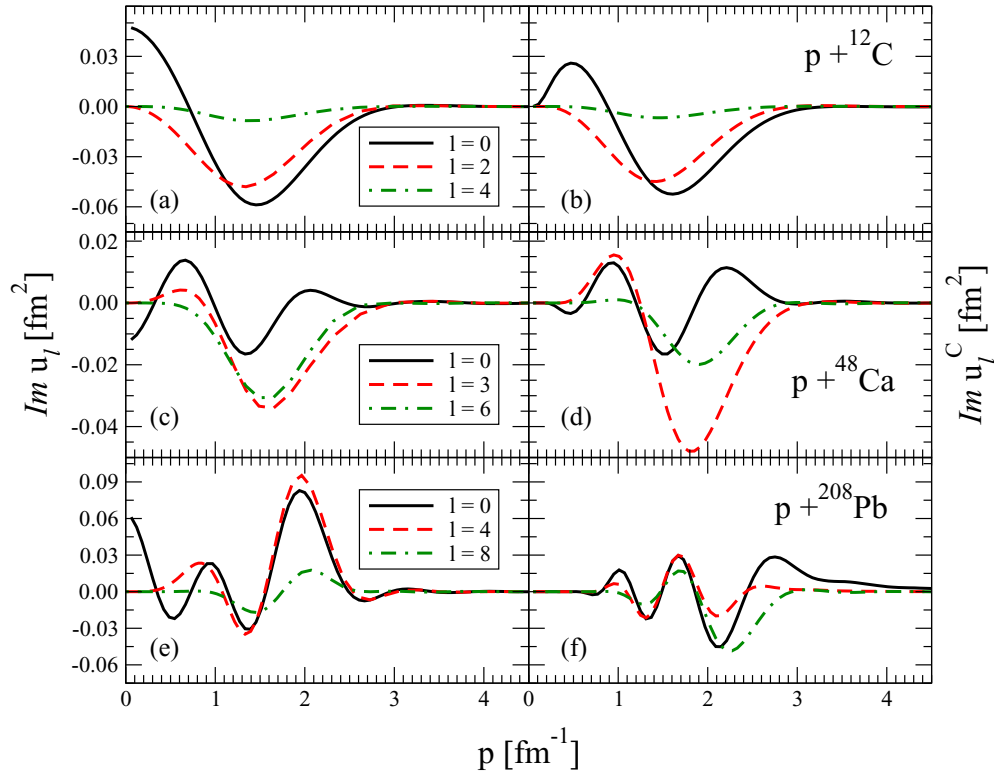


FIG. 4. (Color online) Same as Fig. 3, but for the imaginary parts of the nuclear form factors $u_l(p)$ (left panels) and Coulomb-distorted nuclear form factors $u_l^C(p)$ (right panels).

under consideration, the nuclear form factor goes to zero already at 3 to 4 fm^{-1} . This is a property of the underlying Woods-Saxon ansatz. This is clearly different from the results shown in Sec. III A for the Yamaguchi-type form factor, which at those momenta is still near its maximum values. This feature turns out to be important in the efficiency of our calculations, since it reduces the required grid sizes for the integration.

The imaginary parts of $u_l^C(p)$ exhibit features similar to the real parts. Because the original optical potentials contain an important imaginary component, which accounts for the absorption to all the nonelastic channels in the scattering process, the magnitude of the imaginary parts shown in Fig. 4 are as relevant as the real parts. This, of course, was not the case for the Yamaguchi form factors of Fig. 1. As for the real parts, the number of partial waves with a significant $\text{Im}[u_l^C(p)]$ increases with the size of the system, and, the higher the charge of the target nucleus, the larger is the momentum shift away from zero momentum of the structure of the form factor. We choose to show the form factors only for momenta up to 4.5 fm^{-1} . However, we should point out that, the larger the charge is, the further out in momenta one has to go before the Coulomb-distorted form factor approaches the pure nuclear one within, e.g., three significant figures. In the case of ^{12}C , this occurs at about 4–5 fm^{-1} , whereas for ^{48}Ca one has to go out to 5–6 fm^{-1} . For ^{208}Pb , this occurs beyond 8 fm^{-1} .

Since there is a qualitative difference between the Yamaguchi form factor studied in Sec. III A and the more realistic ones for heavy nuclei, we see it warranted to again carefully study the role of the pole region in the integral of Eq. (4). We again perform the integration, but we leave out a

region of momenta around the pole $q \in [p - \Delta, p + \Delta]$ when computing the integral. In Fig. 5 we compare the complete calculation of the real part of the $l = 0$ Coulomb-distorted form factor $u_0^C(p)$, for $p + ^{12}\text{C}$, with calculations of the same integral in which a region Δ around the pole at p was removed. In Fig. 6 we show the identical calculations for the real part of the $l = 0$ form factor, but now for the $p + ^{208}\text{Pb}$ form factor.

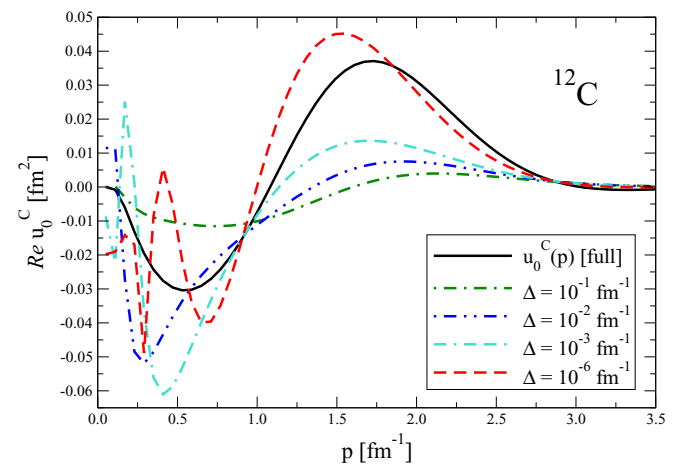


FIG. 5. (Color online) The real part of the $l = 0$ Coulomb-distorted nuclear form factors $u_0^C(p)$ as function of the external momentum p for ^{12}C at $E_{\text{cm}} = 30$ MeV. The solid (black) line shows the full results, while for all other curves an interval of the size Δ has been cut out left and right of the pole p while performing the integration.

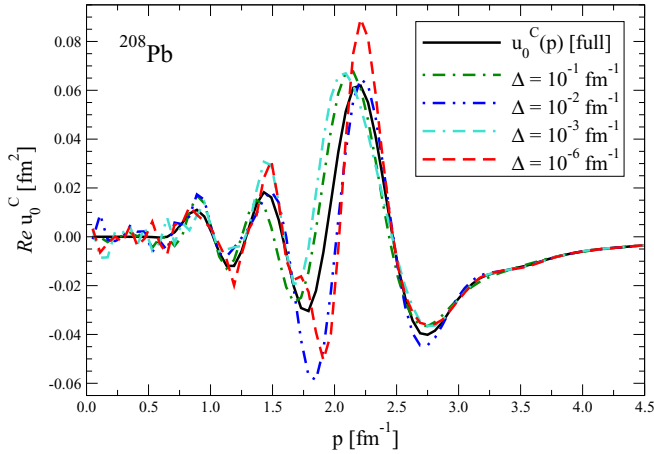


FIG. 6. (Color online) The real part of the $l=0$ Coulomb-distorted nuclear form factors $u_0^C(p)$ as function of the external momentum p for ^{208}Pb at the fixed support point $E_{\text{cm}} = 36$ MeV. The solid (black) line shows the full results, while for all other curves an interval of the size Δ has been cut out left and right of the pole p while performing the integration.

We find that for large Δ (say $\Delta = 0.1 \text{ fm}^{-1}$) the form factor has little resemblance to the exact one. As Δ becomes smaller, there is an approach to the mean value but with shorter and shorter periods, a characteristic feature of Fourier transforms.

To obtain some qualitative insight into this behavior, one has to consider the functional form of the Coulomb wave function $\psi_{l,p}^C(q)$, and particularly its dependence on the Sommerfeld parameter η . For small η , the Coulomb wave function is more evenly distributed around the pole $q = p$ and there are important cancellations. This is the case of $p + ^{12}\text{C}$ shown in Fig. 5. In the case of $p + ^{208}\text{Pb}$, shown in Fig. 6, η is large and $\psi_{l,p}^C(q)$ is much larger for $q < p$ than for $q > p$. Consequently, cancellation effects are smaller and one is not as sensitive to Δ . As Figs. 5 and 6 clearly demonstrate, it is of utmost importance to carefully treat the pole region in the integral of Eq. (4), since major contributions to this integral come from the region around the pole.

IV. SUMMARY AND DISCUSSION

In this work we developed numerical methods to obtain the Coulomb-distorted nuclear form factors in momentum space, which will serve as a basis for Faddeev-AGS three-body calculations of (d, p) reactions. First, we tested our implementation for Yamaguchi form factors, which have been widely used by the few-body community. Our implementations were compared to results obtained with the MATHEMATICA[®] [26] software and we achieved agreement of at least six significant figures in the Coulomb-distorted form factors. Next, we used a multirank separable nuclear interaction built from phenomenological optical potentials using a generalized EST scheme. The resulting Coulomb-distorted form factors differed considerably from those obtained with the Yamaguchi form, particularly in the momentum tail, which for the realistic interaction is strongly reduced. The general effect of the Coulomb force is to shift the structure of the form factors away

from zero momentum. We also considered the dependence of the resulting Coulomb-distorted form factors on angular momentum and external momentum, as both are relevant to the applications we have in mind.

Now that a numerically feasible method has been developed to calculate Coulomb-distorted nuclear form factors, we need to think of a test case, preferably in the two-body system, where we can compare our calculation with an independently obtained coordinate-space calculation. Calculations of elastic scattering of protons from nuclei with local as well as nonlocal folding optical potentials in momentum space have relied either on screening techniques [29] or on solving the Lippmann-Schwinger equation in the Coulomb basis [30,31] to avoid screening. However, the integral equation for elastic scattering in the momentum-space Coulomb basis for an arbitrary potential $v_l(p', p)$ leads to a pinch singularity when both momenta p' and p approach the on-shell external momentum at the same time. In Refs. [30,31] this problem was circumvented by calculating the Coulomb distortions in coordinate space and then carrying out a Fourier transform to momentum space.

Inspired by the work of [18] and [32], we considered an example in which we can compare our momentum calculation with a corresponding coordinate-space calculation. In Ref. [18], proton elastic scattering from ^{12}C and ^{16}O is studied with a rank-1 separable potential. In Ref. [32], proton-proton (pp) elastic scattering is considered with a separable potential of rank 2. In both cases Yamaguchi-type form factors are used, only low angular momenta are calculated, and Yamaguchi parameters are fitted to describe experimentally extracted proton phase shifts. The form factors we employed in Sec. III are derived within a generalized EST scheme [19] and are essentially the half-shell $n - A$ t matrices calculated from the CH89 phenomenological global optical potential [24]. If we intend to compare our momentum-space calculation with a corresponding coordinate-space calculation, we need to identify situations in which not only on-shell but also off-shell t matrices of the CH89 and its separable representation are reasonably close to each other. The off-shell t matrices for $l = 0, 1, 2, 3$ obtained with the EST scheme are too different from those of the original CH89 interaction to be used as test cases. For this reason, we considered the partial waves $l = 4$ through $l = 10$ for proton elastic scattering from ^{48}Ca at 38 MeV laboratory kinetic energy, and we used the formulation that was described in Ref. [32] to compute S matrices using our Coulomb-distorted momentum-space basis. For this calculation one needs to integrate over the external momentum of the Coulomb wave function. Figure 7 shows the real (a) and imaginary (b) parts of the partial-wave S matrices corresponding to $J = L + 1/2$, as a function of angular momentum. The coordinate-space calculations including the Coulomb interaction are represented by crosses, while the results of our momentum-space calculations are given by pluses. For reference, we also show the coordinate-space calculation when the Coulomb force is switched off (solid circles). By comparing the coordinate-space calculation with and without the Coulomb force, we can see that Coulomb distortions are still important up to $l = 8$. In those cases the momentum-space calculation taking into account Coulomb

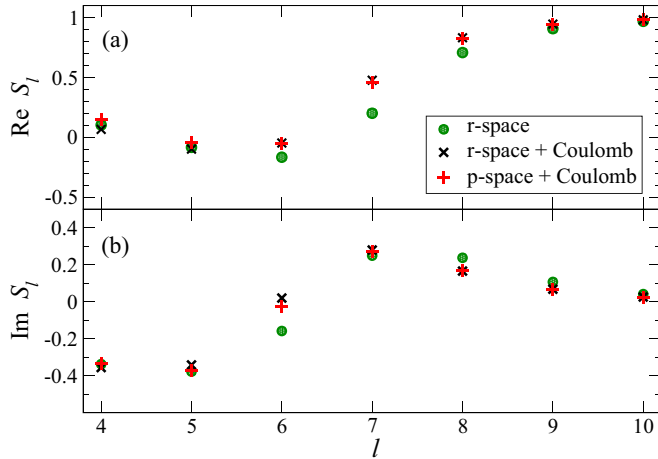


FIG. 7. (Color online) The real (a) and imaginary (b) parts of the partial-wave S matrix $S_{L+1/2}$, for the $p + {}^{48}\text{Ca}$ system obtained from the CH89 [24] phenomenological optical potential as a function of the angular momentum l at a projectile incident kinetic energy of 38 MeV. The solid (green) circles indicate the coordinate-space calculation for which the contribution due to the Coulomb force is omitted. The (black) X symbols correspond to the coordinate-space calculation including the Coulomb force. The (red) + symbols give the momentum-space calculation based on the separable representation of the CH89 potential [19] including the Coulomb force.

distortions agrees with the corresponding coordinate-space calculation. This gives us further confidence that our numerical calculations of Coulomb-distorted form factors are correct and reliable.

Since our form factors are half-shell two-body t matrices obtained as solutions of a momentum-space Lippman-Schwinger equation, they do not contain parameters that can be adjusted to reproduce the phase shifts as was done in Ref. [32]. If one wanted to apply an EST scheme in order to describe proton elastic scattering, one would need to start from the solution of the Lippmann-Schwinger equation, as was done in Ref. [30], to obtain the Coulomb-distorted half-shell t matrices which enter an EST scheme. However, elastic proton scattering is not the focus of this work, and therefore we are satisfied with the consistency checks for selected situations, as well as the checks described in Sec. III A.

To our knowledge, this is the first time that Coulomb-distorted realistic nucleon-nucleus form factors have been computed in the context of separable interactions. A major challenge in solving this problem is the nature of the oscillatory singularity due to the momentum-space Coulomb wave function. We implemented an appropriate method to handle the singularity and have studied carefully the impact in our calculations.

Our results demonstrate that we are able to accurately compute the integrals leading to the Coulomb-distorted form factors. Now that these challenging form factors have been obtained, they can be introduced into the Faddeev-AGS equations to solve the three-body problem without resorting to screening. Our expectation is that solutions to the Faddeev-AGS equations written in the Coulomb-distorted basis can be

obtained for a large variety of $n + p + A$ systems, without a limitation on the charge of the target. From those solutions, observables for (d, p) transfer reactions should be readily calculated. Work along these lines is now in progress.

ACKNOWLEDGMENTS

The TORUS Collaboration acknowledges the inspiration and insight of Prof. Akram Mukhamedzhanov with respect to this project. Upadhyay and Eremenko are grateful to Prof. Akram Mukhamedzhanov and Dr. Ahdior Sattarov for providing invaluable guidance in the early stages of this work. Hlophe thanks Prof. Steve Weppner for his support in developing a separable representation of the optical potential for ${}^{12}\text{C}$. The authors are also grateful to Prof. Ron Johnson and Prof. Jeff Tostevin for many useful discussions. This work was performed in part under the auspices of the US Department of Energy under the topical collaborations in nuclear theory program No. DE-SC0004084 and No. DE-SC0004087 (TORUS Collaboration), under Contracts No. DE-FG52-08NA28552 with Michigan State University and No. DE-FG02-93ER40756 with Ohio University, by Lawrence Livermore National Laboratory under Contract No. DE-AC52-07NA27344, and U.T. Battelle LLC Contract No. DE-AC0500OR22725. F.M. Nunes also acknowledges support from the National Science Foundation under Grant No. PHY-0800026. This research used resources from the Michigan State University High Performance Computing Center and the National Energy Research Scientific Computing Center, which is supported by the Office of Science of the US Department of Energy under Contract No. DE-AC02-05CH11231.

APPENDIX A: PARTIAL-WAVE COULOMB WAVE FUNCTION IN MOMENTUM SPACE

A closed analytic form for the Coulomb function in momentum space was first presented in Ref. [33] and introduced in the field of nuclear reactions by Dolinskii *et al.* [14], where also its partial-wave decomposition was introduced. In this Appendix we discuss specific aspects regarding our implementation of these Coulomb functions.

The procedure starts with the Fourier transform of the Coulomb wave function in coordinate space. For our work, the most convenient final expression is given in Eq. (A.2) of Ref. [14]:

$$\psi_p^C(\vec{q}) = -4\pi \exp^{-\eta\pi/2} \Gamma(1 + i\eta) \times \lim_{\gamma \rightarrow +0} \frac{d}{d\gamma} \left\{ \frac{[q^2 - (p + i\gamma)^2]^{i\eta}}{[\gamma^2 + |\vec{q} - \vec{p}|^2]^{1+i\eta}} \right\}, \quad (\text{A1})$$

where $\vec{q} = q \hat{q}$. It should be pointed out that the definition of the Fourier transform of Eq. (A1) differs from the one in Ref. [14] by a factor of $1/(2\pi)^3$.

Following Ref. [14], one performs the partial-wave decomposition and, after some nontrivial mathematical manipulations, obtains the expression of Eq. (1). The expression in Eq. (1) is the most general explicit form of the partial-wave Coulomb wave function in momentum space.

Unfortunately, this general form does not allow a direct numerical implementation and analysis due to the nature of the spherical functions $Q_l^{i\eta}(\zeta)$. Following Ref. [14], the spherical functions can be expressed in terms of the hypergeometric functions ${}_2F_1(a, b; c; z)$. These hypergeometric functions depend on the angular momentum l , the strength of the Coulomb potential η , and a dynamic variable related to the momenta ζ as defined below Eq. (1).

For $\zeta \approx 1$ we use Eq. (8.773.2) from Ref. [34],

$$\begin{aligned} Q_l^{i\eta}(\zeta) = & \frac{e^{-\pi\eta}}{2} \left\{ \Gamma(i\eta) \left(\frac{\zeta+1}{\zeta-1} \right)^{i\eta/2} \right. \\ & \times {}_2F_1 \left(-l, l+1; 1-i\eta; \frac{1-\zeta}{2} \right) \\ & + \Gamma(-i\eta) \frac{\Gamma(l+i\eta+1)}{\Gamma(l-i\eta+1)} \left(\frac{\zeta-1}{\zeta+1} \right)^{i\eta/2} \\ & \left. \times {}_2F_1 \left(-l, l+1; 1+i\eta; \frac{1-\zeta}{2} \right) \right\}. \quad (\text{A2}) \end{aligned}$$

This expression is consistent with that presented in Eq. (21) of Ref. [14]. Note however that, to improve the numerical accuracy, we transform this hypergeometric functions using Eq. (9.131.1) from Ref. [34]. This transform leads to stable and faster computation of the hypergeometric functions for $\zeta \approx 1$.

The constraint $\zeta \approx 1$ translates to the condition $q \approx p$. However, when p and q are sufficiently different, then $\zeta \gg 1$, and Eq. (A2) is not valid. In this situation we have to consider an alternate expansion, namely, Eq. (8.703) of [34], which is given as

$$\begin{aligned} Q_l^{i\eta}(\zeta) = & \frac{e^{-\pi\eta} \Gamma(l+i\eta+1) \Gamma(1/2)}{2^{l+1} \Gamma(l+3/2)} (\zeta^2-1)^{i\eta/2} \zeta^{-l-i\eta-1} \\ & \times {}_2F_1 \left(\frac{l+i\eta+2}{2}, \frac{l+i\eta+1}{2}; l+\frac{3}{2}; \frac{1}{\zeta^2} \right). \quad (\text{A3}) \end{aligned}$$

From Fig. 8, it can be seen that Eq. (A3) is well behaved at low and high momenta, where the original expression Eq. (A2) is ill defined. Equation (A2) is valid around the singularity point $q = p$. Thus, it is important to switch to the appropriate expansion depending on the value of ζ .

This switch should happen when the fourth arguments of the hypergeometric functions in the two different expansions are equal:

$$\frac{1}{\zeta^2} = \frac{\zeta-1}{\zeta+1}. \quad (\text{A4})$$

This equation has only one real root: $\zeta = 1.83928655 \dots$. It is better to have this condition formulated in terms of p and q . From the definition of ζ , we obtain

$$q_{1,2} = (\zeta \mp \sqrt{\zeta^2-1})p. \quad (\text{A5})$$

Good estimates for the roots of this implicit equation are $q_1 \approx 0.3p$ and $q_2 \approx 3.4p$. Since the two expansions of $Q_l^{i\eta}(\zeta)$ are equally valid around the transition points, our implementation uses these estimates. More details can be found in Ref. [35].

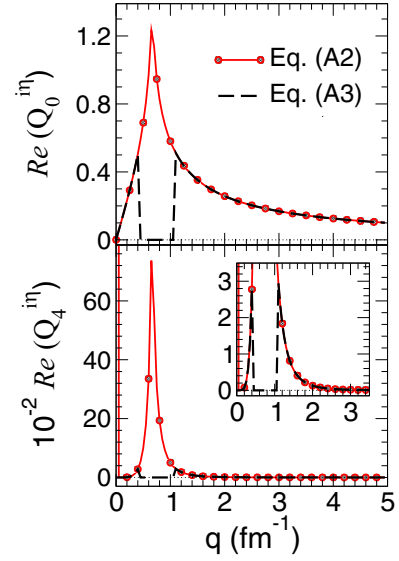


FIG. 8. (Color online) Comparison of two expansions of the spherical function $Q_l^{i\eta}(\zeta)$ as a function of momentum. Results are shown for the real part of $Q_l^{i\eta}(\zeta)$ with parameters evaluated for ^{12}C at $p = 0.67 \text{ fm}^{-1}$, for $l = 0$ (top panel) and $l = 4$ (lower panel).

APPENDIX B: THE REGULARIZATION PROCEDURE

The difficulty with handling the singularity of Eq. (6) was clearly indicated in Ref. [6]. Therein the idea of using the Gel'fand and Shilov regularization was introduced. In this Appendix, we generalize the formulation of Ref. [6] for complex functions and present a detailed description of the method, bearing in mind our physical applications.

1. General formulation of the Gel'fand and Shilov regularization

When calculating matrix elements in the Coulomb basis, one encounters integrals of the following form, containing a singular point at $x = 0$:

$$I = \lim_{\gamma \rightarrow 0} \int_{-\Delta}^{\Delta} \frac{\phi(x) dx}{(x \pm i\gamma)^{1 \pm i\eta}} \equiv \int_{-\Delta}^{\Delta} \frac{\phi(x) dx}{(x \pm i0)^{1 \pm i\eta}}, \quad (\text{B1})$$

where $\phi(x)$ is a smooth, well-defined function in the domain $x \in [-\Delta, \Delta]$, and $\phi(0) \neq 0$, $\phi'(0) \neq 0$. The leading singularity of the integrand is given by

$$S_{\pm}(x) = \frac{1}{(x \pm i0)^{1 \pm i\eta}}. \quad (\text{B2})$$

The exponent $1 \pm i\eta$ in the denominator of Eq. (B2) leads to oscillations with an amplitude increasing to infinity and a period limiting to 0, as $x \rightarrow 0$. Thus, in order to compute the integral I , one has to regularize it.

By using the regularization scheme proposed by Gel'fand and Shilov [25], the integral from 0 to Δ can be written as

$$\begin{aligned} \int_0^{\Delta} \frac{\phi(x) dx}{(x \pm i0)^{1 \pm i\eta}} &= \int_0^{\Delta} \frac{\phi(x) dx}{x^{1 \pm i\eta}} \\ &= \int_0^{\Delta} dx \frac{\phi(x) - \phi(0) - \phi'(0)x}{x^{1 \pm i\eta}} \\ &\quad \pm \frac{i\phi(0)}{\eta} \Delta^{\mp i\eta} + \frac{\phi'(0)}{1 \mp i\eta} \Delta^{1 \mp i\eta}. \quad (\text{B3}) \end{aligned}$$

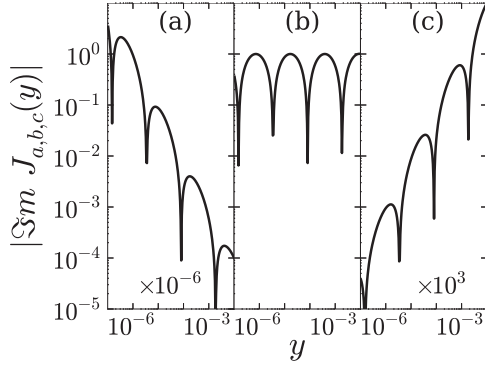


FIG. 9. The singularity $|\Im m[J_{a,b,c}(y)]|$ according to Eq. (B2) near the on-shell point $y = 0$: (a) unregularized, (b) with principal value regularization, and (c) with Gel'fand-Shilov regularization. The precise definition of the function $J_{a,b,c}(y)$ in each panel is defined in the text.

Noticing that

$$\frac{1}{(-x \pm i0)^{1 \pm i\eta}} = \frac{(e^{\mp i\pi})^{\mp i\eta}}{x^{1 \pm i\eta}} = \frac{e^{-\pi\eta}}{x^{1 \pm i\eta}} \quad \text{for } (x > 0) \quad (\text{B4})$$

one obtains the following relation:

$$\int_{-\Delta}^0 \frac{\phi(x) dx}{(x \pm i0)^{1 \pm i\eta}} = -e^{-\pi\eta} \int_0^{\Delta} \frac{\phi(x) dx}{x^{1 \pm i\eta}}. \quad (\text{B5})$$

This leads to the following expression for the integral I :

$$I = (1 - e^{-\pi\eta}) \left[\int_0^{\Delta} dx \frac{\phi(x) - \phi(0) - \phi'(0)x}{x^{1 \pm i\eta}} \pm \frac{i\phi(0)}{\eta} \Delta^{\mp i\eta} + \frac{\phi'(0)}{1 \mp i\eta} \Delta^{1 \mp i\eta} \right]. \quad (\text{B6})$$

Now, all terms in Eq. (B6) are regular; i.e., the integral I is regularized and well behaved.

The effect of the regularization procedure is illustrated in Fig. 9, where we plot the magnitude of the imaginary part of the first integrand in Eq. (B6) at different stages of the regularization. For this illustration, $\phi(y) = 1 + y + y^2$ so that $\phi(0) = 1$ and $\phi'(0) = 1$, where y is dimensionless. In Fig. 9(a), the unregularized function $J_a(y) \equiv \phi(y)S_+(y)$ is presented. Figure 9(b) then shows the behavior of $J_b(y) \equiv \{\phi(y) - \phi(0)\}S_+(y)$, i.e., the behavior when the singular point is subtracted. The amplitude of the oscillations now is finite, but the integral is still irregular. In Fig. 9(c) the behavior of the fully regularized integrand $J_c(y) \equiv \{\phi(y) - \phi(0) - \phi'(0)y\}S_+(y)$ is presented. Though the oscillations are still present, the amplitude is linearly decreasing, making the integral sums for this integrand converge monotonically with increasing number of points (terms). Thus, the corresponding integral becomes regular.

In case Δ is small, Eq. (B6) may be simplified. The first term becomes of $O(\Delta^2)$, and the last one of $O(\Delta)$. By neglecting both of them, one gets

$$I|_{\Delta \rightarrow 0} \approx \pm i(1 - e^{-\pi\eta})\phi(0)\Delta^{\mp i\eta}\eta. \quad (\text{B7})$$

This expression is used in our implementation.

2. Application to integrals involving the Coulomb wave function in momentum space

Around the point $q = p$, rearranging Eq. (A2), one can write the wave function $\psi_{l,p}^C(q)$ in the following form:

$$\psi_{l,p}^C(q) = \mathcal{A}(p,l,\eta) \left[\frac{\mathcal{B}(q,p,l,\eta)}{(q-p+i0)^{1+i\eta}} - \frac{\mathcal{B}(q,p,l,\eta)^*}{(q-p-i0)^{1-i\eta}} \right], \quad (\text{B8})$$

where the auxiliary functions are defined as

$$\begin{aligned} \mathcal{A}(p,l,\eta) &= 2\pi i \exp(i\sigma_l - \pi\eta/2)/(4p)^l, \\ \mathcal{B}(q,p,l,\eta) &= \Gamma(1+i\eta) \exp(-i\sigma_l)(q+p)^{2l-1+i\eta} q^{-(l+1)} \\ &\quad \times {}_2F_1(-l, -l-i\eta; 1-i\eta; \rho(q,p)), \\ \rho(q,p) &= (q-p)^2(q+p)^2, \\ \exp(2i\sigma_l) &= \frac{\Gamma(l+1+i\eta)}{\Gamma(l+1-i\eta)} \quad \text{so } \sigma_l = \arg \Gamma(l+1+i\eta). \end{aligned} \quad (\text{B9})$$

Note that, apart from the Coulomb phase $\exp(i\sigma_l)$, the Coulomb wave function $\psi_{l,p}^C(q)$ is a real-valued function. From Eq. (B8) one can see that the wave function $\psi_{l,p}^C(q)$ is singular at the point $q = p$ with the leading singularity $S_{\pm}(x)$ as in Eq. (B2), where

$$x = p - q. \quad (\text{B10})$$

Thus, we consider a function $\mathcal{F}_l(p)$,

$$\mathcal{F}_l(p) = \frac{1}{2\pi} (I_0^{p-\Delta} + I_{p-\Delta}^{p+\Delta} + I_{p+\Delta}^{\infty}), \quad (\text{B11})$$

where

$$I_a^b = \int_a^b dq q^2 f_l(q) \psi_{l,p}^C(q). \quad (\text{B12})$$

For the applications of Sec. III, $f_l(q) \in \mathbb{C}$ is a smoothly varying function of q . The singular behavior of the wave function $\psi_{l,p}^C(q)$ must be addressed when computing $\mathcal{F}_l(p)$. Since this singularity only causes a problem in some region around $q = p$, we now focus on this specific region. For the remaining part of the Appendix, only the integral $I_{p-\Delta}^{p+\Delta}$ will be discussed, namely,

$$\begin{aligned} I_{p-\Delta}^{p+\Delta} &= \mathcal{A}(p,l,\eta) \int_{p-\Delta}^{p+\Delta} dq q^2 f_l(q) \\ &\quad \times \left[\frac{\mathcal{B}(q,p,l,\eta)}{(q-p+i0)^{1+i\eta}} - \frac{\mathcal{B}(q,p,l,\eta)^*}{(q-p-i0)^{1-i\eta}} \right]. \end{aligned} \quad (\text{B13})$$

By introducing

$$\varphi(x) = (p-x)^2 \mathcal{B}(p-x,p,l,\eta), \quad (\text{B14})$$

and changing variables to $x = p - q$ in the denominators,

$$\begin{aligned} \frac{1}{(q-p+i0)^{1+i\eta}} &= \frac{(e^{i\pi})^{-1-i\eta}}{(x+i0)^{1+i\eta}} = \frac{-e^{\pi\eta}}{(x+i0)^{1+i\eta}}, \\ \frac{1}{(q-p-i0)^{1-i\eta}} &= \frac{(e^{-i\pi})^{-1+i\eta}}{(x-i0)^{1-i\eta}} = \frac{-e^{\pi\eta}}{(x-i0)^{1-i\eta}}, \end{aligned} \quad (\text{B15})$$

the integral splits into two terms,

$$I_{p-\Delta}^{p+\Delta} = -\mathcal{A}(p, l, \eta) e^{\pi\eta} \left[\int_{-\Delta}^{\Delta} dx \frac{f_l(p-x)\varphi(x)}{(x+i0)^{1+i\eta}} - \int_{-\Delta}^{\Delta} dx \frac{f_l(p-x)\varphi^*(x)}{(x-i0)^{1-i\eta}} \right]. \quad (\text{B16})$$

If in Eq. (B16) we consider $f_l(p-x)$ to be a real function, then the second term in square brackets in Eq. (B16) becomes the complex conjugate of the first. Because $z - z^* = 2i \Im z$, the number of integrals to be regularized and computed in Eq. (B16) is then reduced to one. In order to arrive at Eq. (A12) of Ref. [6], one needs to replace $f_l(q)$ by the Yamaguchi form factor and apply Eq. (B6).

In this work we focus on complex form factors $f_l(q) \in \mathbb{C}$. In this case both terms in Eq. (B16) must be treated separately. This means Eq. (B6) is applied twice, so we obtain

$$\begin{aligned} I_{p-\Delta}^{p+\Delta} = \mathcal{A}(p, l, \eta) (1 - e^{\pi\eta}) & \left\{ \int_0^{\Delta} dx \frac{f_l(p-x)\varphi(x) - f_l(p)\varphi(0) - [f_l'(p)\varphi(0) + f_l(p)\varphi'(0)]x}{x^{1+i\eta}} + \frac{if_l(p)\varphi(0)}{\eta} \Delta^{-i\eta} \right. \\ & + \frac{f_l'(p)\varphi(0) + f_l(p)\varphi'(0)}{1-i\eta} \Delta^{1-i\eta} - \int_0^{\Delta} dx \frac{f_l(p-x)\varphi^*(x) - f_l(p)\varphi^*(0) - [f_l'(p)\varphi^*(0) + f_l(p)(\varphi^*)'(0)]x}{x^{1-i\eta}} \\ & \left. + \frac{if_l(p)\varphi^*(0)}{\eta} \Delta^{i\eta} - \frac{f_l'(p)\varphi^*(0) + f_l(p)(\varphi^*)'(0)}{1+i\eta} \Delta^{1+i\eta} \right\}. \quad (\text{B17}) \end{aligned}$$

To further simplify Eq. (B17), we proceed in a similar fashion as done in Eq. (B7). By choosing Δ small enough (e.g., 10^{-6} fm^{-1}), we obtain

$$I_{p-\Delta}^{p+\Delta} = \frac{i}{\eta} \mathcal{A}(p, l, \eta) (1 - e^{\pi\eta}) f_l(p) [\varphi(0)\Delta^{-i\eta} + \varphi^*(0)\Delta^{i\eta}] = \frac{2i}{\eta} \mathcal{A}(p, l, \eta) (1 - e^{\pi\eta}) f_l(p) p^2 \Re\{ \mathcal{B}(p, p, l, \eta) \Delta^{-i\eta} \}. \quad (\text{B18})$$

Note that $\mathcal{B}(p, p, l, \eta)$ has a simple form because $\rho(p, p) = 0$. The expression Eq. (B18) is finally used to compute the regularized part of the integral of Eq. (B13). For the physical applications we discuss in the main text, $\{\mathcal{F}_l = [u_l^C]^*, f_l = u_l^*\}$ or $\{\mathcal{F}_l = u_l^C, f_l = u_l\}$.

-
- [1] I. J. Thompson and F. M. Nunes, *Nuclear Reactions for Astrophysics: Principles, Calculation and Applications of Low-Energy Reactions* (Cambridge University Press, Cambridge, England, 2009).
- [2] F. M. Nunes and A. Deltuva, *Phys. Rev. C* **84**, 034607 (2011).
- [3] K. Schmitt *et al.*, *Phys. Rev. Lett.* **108**, 192701 (2012).
- [4] R. Kozub *et al.*, *Phys. Rev. Lett.* **109**, 172501 (2012).
- [5] F. Nunes and N. Upadhyay, *J. Phys. G: Conf. Ser.* **403**, 012029 (2012).
- [6] A. M. Mukhamedzhanov, V. Eremenko, and A. I. Sattarov, *Phys. Rev. C* **86**, 034001 (2012).
- [7] A. Deltuva, *Phys. Rev. C* **88**, 011601 (2013).
- [8] A. Deltuva, A. M. Moro, E. Cravo, F. M. Nunes, and A. C. Fonseca, *Phys. Rev. C* **76**, 064602 (2007).
- [9] N. J. Upadhyay, A. Deltuva, and F. M. Nunes, *Phys. Rev. C* **85**, 054621 (2012).
- [10] A. Deltuva and A. C. Fonseca, *Phys. Rev. C* **79**, 014606 (2009).
- [11] E. Alt, P. Grassberger, and W. Sandhas, *Nucl. Phys. B* **2**, 167 (1967).
- [12] A. Deltuva, A. C. Fonseca, and P. U. Sauer, *Phys. Rev. C* **71**, 054005 (2005).
- [13] A. Deltuva, A. C. Fonseca, and P. U. Sauer, *Phys. Rev. C* **72**, 054004 (2005).
- [14] E. I. Dolinskii and A. M. Mukhamedzhanov, *Yad. Fizika* **3**, 252 (1966) [*Sov. J. Nucl. Phys.* **3**, 180 (1966)].
- [15] H. van Haeringen and L. Kok, Delft University of Technology Report THD-A-ST 80-08, 1980 (unpublished).
- [16] K. Dreissigacker, H. Popping, P. Sauer, and H. Walliser, *J. Phys. G* **5**, 1199 (1979).
- [17] G. Cattapan, G. Pisent, and V. Vanzani, *Z. Phys. A* **274**, 139 (1975).
- [18] G. Cattapan, G. Pisent, and V. Vanzani, *Nucl. Phys. A* **241**, 204 (1975).
- [19] L. Hlophe *et al.* (TORUS Collaboration), *Phys. Rev. C* **88**, 064608 (2013).
- [20] M. Yamaguchi, H. Kamada, and W. Gloeckle, *Few Body Syst.* **54**, 1629 (2013).
- [21] A. Mukhamedzhanov (private communication).
- [22] J. Haidenbauer, Y. Koike, and W. Plessas, *Phys. Rev. C* **33**, 439 (1986).
- [23] J. Haidenbauer and W. Plessas, *Phys. Rev. C* **27**, 63 (1983).
- [24] R. Varner, W. Thompson, T. McAbee, E. Ludwig, and T. Clegg, *Phys. Rep.* **201**, 57 (1991).
- [25] I. Gel'fand and G. Shilov, *Generalized Functions, Volume 1: Properties and Operations* (Academic, New York, 1964).
- [26] W. Research, MATHEMATICA, Version 8.0, Champaign, Illinois, 2010.
- [27] S. P. Weppner, R. B. Penney, G. W. Diffendale, and G. Vittorini, *Phys. Rev. C* **80**, 034608 (2009).
- [28] A. Koning and J. Delaroche, *Nucl. Phys. A* **713**, 231 (2003).
- [29] N. Ottenstein, E. E. van Faassen, J. A. Tjon, and S. J. Wallace, *Phys. Rev. C* **43**, 2393 (1991).
- [30] C. R. Chinn, C. Elster, and R. M. Thaler, *Phys. Rev. C* **44**, 1569 (1991).
- [31] C. Elster, L. C. Liu, and R. M. Thaler, *J. Phys. G* **19**, 2123 (1993).
- [32] W. A. Schnizer and W. Plessas, *Phys. Rev. C* **41**, 1095 (1990).
- [33] E. Guth and C. J. Mullin, *Phys. Rev.* **83**, 667 (1951).
- [34] I. Gradshteyn, I. Ryzhik, and A. Jeffrey, *Tables of Integral, Series, and Products, 5th ed.* (Academic, New York, 1994).
- [35] V. Eremenko *et al.* (TORUS Collaboration), *Comput. Phys. Comm.* (submitted).